Solid-State NMR Investigation of Paramagnetic Nylon-6 Clay Nanocomposites. 1. Crystallinity, Morphology, and the Direct Influence of Fe^{3+} on Nuclear Spins

D. L. VanderHart,[*,†] A. Asano,[‡] and J. W. Gilman[§]

National Institute of Standards and Technology, Gaithersburg, Maryland 20899-8544

Several exfoliated nylon-6/clay nanocomposites (NnC's) were investigated and compared with pure nylon-6 using solid-state NMR, both proton and ^{13}C. NnC's had nominally 5 mass % clay and were generated both by blending and by in situ polymerization (IsP). Most of the studied NnC's contained layered, naturally occurring montmorillonite clays having non-stoichiometric amounts of nonexchangeable Mg^{2+} and Fe^{3+} ions that substitute into octahedral Al^{3+} sites along the midplane of the 1-nm-thick clay layers. The Fe^{3+} ions impart a useful paramagnetism to the clay. Each Mg^{2+} ion leaves an embedded negative charge that must be neutralized with some cation at the surface of the clay. All clays were initially treated with a cationic so-called organic modifier (OM), often a substituted ammonium ion, which increases the clay layer spacing, attaching ionically to the surface of the clay layers. Clay is found to promote growth of the γ-crystalline phase of nylon-6 for both blended and IsP NnC's; α-crystallites are characteristic of the pure nylon-6. Stability of the γ-phase to annealing at 214 °C was investigated. Conversion of γ- to α-crystallinity during annealing was minimal, except for an injection-molded IsP NnC, which had been exposed to a temperature of 295 °C during molding. This high processing temperature produced an irreversible change. An attempt was made to understand, at least qualitatively, the nature of the spectral density of magnetic fluctuations associated with the paramagnetic Fe^{3+} sites in the clay. For this purpose, we looked directly at the influence of Fe^{3+} on the ^{13}C and proton observables in organically modified clays (OMC). We agree with other investigators that the spectral density of paramagnetic fluctuations at the surface of the clay is determined mainly by spin-exchange interactions between Fe^{3+} sites; thus, the spectral density can be altered by changing the Fe^{3+} concentration. Moreover, we find that the spectral density is very wide, having strong contributions all the way from mid-kHz fluctuations to MHz fluctuations near the proton Larmor frequencies. Significant variations in the α/γ ratio were also observed in the injection-molded disk, which reflect either a processing-induced heterogeneity in clay dispersion or a significant variation in cooling history from region to region. Proton spin diffusion and multiple-pulse methods were utilized to compare morphologies for a diamagnetic NnC and nylon-6 with the same thermal histories. Long spacing, crystallinity, and the mobility of the noncrystalline nylon-6 segments are very similar for NnC's and nylon-6.

Introduction

Interest in exfoliated polymer/layered-silicate (clay) nanocomposite (NnC) materials has increased significantly in recent years.[1] The property improvements these materials offer include better mechanical properties,[2] higher heat distortion temperature,[2] better barrier properties,[3] lower water absorption,[4] and reduced flammability.[5] However, additional new characterization techniques are needed to compliment the primary characterization tools currently used to study NnC's: that is, transmission electron microscopy (TEM) and X-ray diffraction (XRD). TEM and XRD are essential for evaluating NnC structure; however, TEM is time-intensive, and only gives qualitative information on the sample as a whole, while low-angle peaks in XRD allow quantification of changes in layer spacing.[6] Typically, however, when layer spacings exceed 6−7 nm in intercalated NnC's or when the layers become relatively disordered in exfoliated NnC's, associated XRD features

---

* To whom correspondence should be addressed.
† Polymers Division.
‡ Polymers Division. Current address is Department of Applied Chemistry, National Defense Academy, 1-10-20 Hashirimizu, Yokosuka 239-8686, Japan.
§ Fire Science Division.
(1) Alexandre, M.; Dubois, P. *Mater. Sci. Eng.(R)* **2000**, *28*, 1.
(2) Kojima, Y.; Usuki, A.; Kawasumi, M.; Okada, A.; Fukushima, Y.; Kurauchi, T.; Kamigaito, O. *J. Mater. Res.* **1993**, *8*, 1185.
(3) Messersmith, P. B.; Giannelis, E. P. *J. Polym. Sci. A., Polym. Chem.* **1995**, *33*, 1047.

(4) Okada, A.; Fukushima, Y.; Kawasumi, M.; Inagaki, S.; Usuki, A.; Sugiyama, S.; Kurauchi, T.; Kamigaito, O. U.S. Patent 4,739,007, 1988.
(5) Gilman, J. W.; Jackson, C. L.; Morgan, A. B.; Harris, R. H.; Manias, E.; Giannelis, E. P.; Wuthenow, M.; Hilton, D.; Phillips, S. *Chem. Mater.* **2000**, *12*, 1866.
(6) Usuki, A.; Kawasumi, M.; Yoshitsugu, K.; Okada, A.; Kurauchi, T.; Kamigaito, O. *J. Mater. Res.* **1993**, *8*, 1174.

weaken to the point of not being useful. However, recent simultaneous SAXS and WAXS studies have yielded quantitative characterization of the mesostructure and crystallite structure in PA-6 clay NnC's.[7] NMR has also been used to characterize NnC's. Yang and Zax determined the relative mobility of bulk and interphase polymer in intercalated PEO NnC's[8] and Mathias et al. the phase structure of PA-6 clay NnC's.[9]

The goal of this study is to determine the capabilities and limitations of solid-state NMR (^{1}H and ^{13}C) as a tool for gaining greater insight about the morphology, surface chemistry, and to a very limited extent, the dynamics of exfoliated polymer clay NnC's. We were especially interested in developing NMR methods to quantify the level of clay exfoliation because we felt that this was an important facet of NnC characterization. We were also interested in the mechanism by which the clay surface both promotes, in melt crystallization, the formation of γ-phase[10,11] crystallites (instead of the α-phase[12] crystallites obtained in the usual melt crystallization of bulk nylon-6) and further stabilizes these crystallites at high annealing temperatures. We also sought ways to probe the stability and fate of the organic modifier, which is applied to the clay prior to introduction of the polymer. Others have investigated the inherent thermal stability of the organically modified clay, but only prior to its incorporation into the NnC's.[13] The integrity of this modifier is not a given considering the high temperatures used in preparing the NnC as well as in processing the NnC. We made a few observations related to the effects of the clay surface on the polymer's dynamic properties, but conclusions were very qualitative. Finally, we also attempted to compare melt-blended nylon-6 clay NnC's with their in situ polymerized (IsP) counterparts using NMR, DSC, and XRD. We submitted a communication[14] that briefly presents some results that pertain to assaying clay dispersion and to monitoring the decomposition of the OM.

This paper is the first of a two-part report on this work. In this paper, we will include DSC results along with NMR results that pertain to issues of morphology and the influence of clay on the nylon-6 crystal forms that develop upon melt crystallization. The stability of these forms to annealing at 214 °C will also be considered. Last, as a lead-in to the second paper, we will discuss and contrast the influence of the paramagnetic Fe^{3+}, embedded within the clay layers, on nuclear spins that are confined in galleries where the maximum distance from a clay surface is only 0.4 nm. A proper understanding of the impact of Fe^{3+} on both the line width and the relaxation behavior of the nearby nuclear spins provides the basis for understanding the pertur-

bation on relaxation of the more distant spins in the NnC's.

In the second paper,[15] we will show how the paramagnetic perturbation on nearby spins allows us to assay the dispersion of clay in families of NnC's and allows us to further examine the stratification of crystallite forms with respect to the clay surfaces. In the second paper, we will also look at issues of chemical stability for certain organic modifiers in blended NnC's.

Experimental Section

Samples. The samples, all in the form of pellets, were obtained from UBE of Yamaguchi, Japan, and from Southern Clay Products of Gonzales, TX. Some characteristics of these samples are collected in Table 1. The nylon-6 ("N6") sample was obtained from Southern Clay and is the material used in the physical melt-blending of the nylon-6/clay NnC's. The designations we apply to the nylon-6/clay samples are as follows: "N6C-*xx-yy*" where N6C in this name refers to nylon-6/clay, *xx* refers to the method of combining the materials (*xx* = "Is" stands for in situ polymerization of the nylon in the presence of the treated clay and *xx* = "B" stands for physical blending). Finally, *yy* refers to the type of treated clay used to make this NnC ("M" stands for paramagnetic, naturally occurring montmorillonite clay (montmorillonite refers to a broad class of layered aluminosilicates with an *average*[16] unit cell formula, $Z^+_{1.03}[Mg_{0.71}Al_{2.98}Fe^{3+}_{0.37}Fe^{2+}_{0.01}(Si_{7.67}Al_{0.32})O_{20^-}(OH)_4]$, and a diameter-to-thickness ratio of roughly 100:1, implying a plate diameter of about 0.1 μm; Z^+ is assumed here to be a monovalent cation but Ca^{2+} is commonly found along with Na^+ and K^+). "L" represents diamagnetic, synthetic Laponite clay. "1" and "2" refer to the different surface treatments (organic modifiers), which can be found in Table 1.

All the NnC samples had a nominal 5% clay composition by mass, where, for the Southern Clay NnC's, the organic modifier is considered part of the clay mass, but for the UBE NnC's, 5% represents the mass of the unmodified clay. Hence, the UBE materials have higher clay loading. Different thermal histories were imposed on all of the samples and these histories are tabulated in Table 1 along with other parameters to be discussed. A lettered suffix is attached to each sample name to distinguish these different histories.

Both melt crystallization under the "slow-cooling" (SC) protocol as well as annealing at 214 °C were performed in a convection oven in sealed glass tubes containing nitrogen gas. The tubes were placed in wells drilled into a brass block. During melt crystallization under the SC protocol, the oven temperature was raised to and held, for about 3 h, at an initial value of 248 °C and then ramped down at 1 °C/min. There is a thermal lag in the cooling inside the block. However, by the time the crystallization of the nylon begins (near 200 °C), the rate of change of the block temperature is close to 1 °C/min, even though the actual oven temperature at any given time is considerably less than the block temperature.

In the process of annealing at 214 °C, the sealed tubes were placed in the brass block in an unheated oven. The oven was then turned on and ramped up at 10 °C/min to the desired temperature, T_{set}. The time of annealing began when the oven reached T_{set}. The temperature inside the block lagged the oven temperature, achieving about (T_{set} − 15 °C) after 1 h and being within 1 °C of T_{set} after 2 h. Therefore, a 2.5-h annealing at 214 °C involved a relatively slow approach to 214 °C and only about 0.5 h in the interval from 213 to 214 °C. With this slow heating, the probability of melting a significant portion of the sample during initial heating is minimized and any changes in crystal habit are then likely to proceed either by solid-state conversion or by the growth of existing crystalline domains. Unless specifically stated otherwise, cooling of the annealed

(7) Lincoln, D. M.; Vaia, R. A.; Wang, Z.-G.; Hsiao, B. S. *Polymer* **2001**, *42*, 1621.

(8) Yang, D.-K.; Zax, D. B. *J. Chem. Phys.* **1991**, *110*, 5325.

(9) Mathias, L. J.; Davis, R. D.; Jarrett, W. L. *Macromolecules* **1999**, *32*, 7958.

(10) Arimoto, H.; Ishibashi, M.; Hirai, M. *J. Polym. Sci. (A)* **1965**, *3*, 317.

(11) Bradbury, E. M.; Brown, L.; Elliott, A.; Parry, D. A. D. *Polymer* **1965**, *6*, 465.

(12) Holmes, D. R.; Bunn, C. W.; Smith, D. J. *J. Polym. Sci.* **1955**, *17*, 159.

(13) Xie, W.; Gao, Z.; Pan, W.; Hunter, D.; Sing, A.; Vaia, R. *Chem. Mater.* **2001**, in press.

(14) VanderHart, D. L.; Asano, A.; Gilman, J. W. *Macromolecules* **2001**, *34*, 3819

(15) VanderHart, D. L.; Asano, A.; Gilman, J. W. *Chem. Mater.* **2001**, *13*, 3796.

Table 1. Sample Information for Nylon-6/Clay Nanocomposites Having Nominally 5 Mass % Clay: Thermal Histories, Paramagnetism (Paramag), Organic Modifier, NMR-Determined Crystallinities (f_c), and Fraction of Crystalline Material that Is α-Phase ($f_α$)

sample[a]	thermal history[b]	paramag?	organic modifier[c]	f_c[d]	$f_α$[e]
N6-a	SC	N	none	0.40	1.00
N6-b	SC/A	N		0.40	1.00
N6C-Is-M-a	IM	Y	12-aminolauric acid	0.33	0.10−0.45
N6C-Is-M-b	IM/A (2.5 h)	Y		0.36	0.67*
N6C-Is-M-c	IM/A	Y		0.41	(0.42−0.75)*
N6C-Is-M-d	IM/SC	Y		0.45	0.10*
N6C-Is-M-e	IM/SC/A	Y		0.45	0.63*
N6C-Is-M-f	SC	Y		0.41	<0.04
N6C-Is-M-g	SC/A (2.5 h)	Y		0.41	<0.07
N6C-Is-M-h	SC/A	Y		0.43	<0.12
N6C-B-L1-a	AR	N	MT(HE)$_2$AI (0.95)	0.36	0.19
N6C-B-L1-b	SC	N		0.42	<0.05
N6C-B-L1-c	SC/A (2.5 h)[f]	N		0.36	0.13
N6C-B-M1-a	AR	Y	HMT$_2$AI (1.25)	0.36	<0.09
N6C-B-M1-b	SC	Y		0.41	<0.02
N6C-B-M1-c	SC/A (2.5 h)	Y		0.38	0.14
N6C-B-M2-a	AR	Y	M$_2$T$_2$AI (1.25)	0.35	<0.15
N6C-B-M2-b	SC	Y		0.40	<0.02
N6C-B-M2-c	SC/A (2.5 h)[f]	Y		0.44	<0.12

[a] Sample abbreviations: nylon-6 (N6), nylon-6/clay nanocomposite (N6C), formation of NnC by in situ polymerization (Is) or physical blending (B), montmorillonite clay (M), Laponite clay (L); numbers refer to different OMs and letters refer to different thermal histories. [b] Abbreviations: "A(*x*)" = annealing at 214 °C for 18 h or for a period, *x*, if explicitly indicated. Samples were taken out of the oven and cooled on the bench after annealing, unless otherwise indicated. "IM" = injection molding at 295 °C into a dye at 80 °C. "SC" is crystallization from the melt at about 250 °C with an oven cooling rate of 1 °C/min. [c] These organic modifiers (OM's) exchange-modify the clay prior to nanocomposite formation. MT(HE)$_2$AI = methyl, hydrogenated-tallow, bis-2-hydroxyethyl, quaternary ammonium ion, HMT$_2$AI is methyl, di(hydrogenated-tallow) ternary ammonium ion and M$_2$T$_2$AI is dimethyl, di(hydrogenated-tallow) quaternary ammonium ion. Numbers in parentheses are the number of equivalents of OM per Kg of clay. The OM is introduced to the clay with chloride counterions except for sulfate counterions used with HMT$_2$AI. [d] NMR crystallinities, based on the relative contribution of the "CR" component of the CPMAS line shape after a CP time of 1 ms. Corrections for differential $T_{1ρ}^H$ decays of the CR and NC protons over that 1 ms are included; corrections decrease the apparent crystallinity values by about 0.03. Standard uncertainties arising from random error are estimated at ±0.03. [e] Based on the relative intensities of the 26.3 ppm (a) and the 34 ppm (γ) lines in the "CR" spectra. Standard uncertainties are estimated at ±0.03; if an * symbol appears next to the value, the standard uncertainty is ±0.05. For the N6C-Is-M-(a,c) samples, ranges are given because 10 different samples were investigated and there was wide variation in $f_α$ (see text). [f] Cooled at 1 °C in oven.

samples was accomplished by opening the oven, while it was at temperature; the tubes were immediately removed and then cooled to ambient temperature in air.

NMR Spectroscopy. Measurements were conducted using two spectrometers, one a noncommercial spectrometer operating at 2.35 T and the other a Bruker Avance 300 spectrometer operating at 7.05 T. The 7.05-T spectrometer became available partway through this study. Some experiments performed at 2.35 T were repeated at the higher field. A few experiments involving direct proton observation were performed only at 7.05 T. We discuss results from both fields because the information to be gained is sometimes more evident from data taken at one of the two fields.

At 2.35 T, 25.2-MHz ^{13}C CPMAS[17] spectra were acquired using a 1-ms cross-polarization (CP) time (unless otherwise noted), a 4.0-kHz magic-angle spinning (MAS) frequency, $ν_r$, and repetition times of 3−5 s. Applied radio frequency fields had amplitudes corresponding to respective nutation frequencies of 59 and 63 kHz for the protons and ^{13}C nuclei. Samples were in the form of machined cylindrical plugs, about 6 mm in diameter and 10−12 mm in length. The method[18] used for separating the signals arising from the crystalline (CR) and the noncrystalline (NC) regions involved different spin-locking times, prior to the fixed CP time. Owing to the different intrinsic rotating-frame relaxation times, $T_{1ρ}^H$, for the protons in the CR and NC regions, the ratio of CR to NC intensity is a function of spin-locking time. Thus, the spectrum of protons in the CR or the NC region can be generated by taking appropriate linear combinations of these spectra. Typically, the two spin-locking times were 0 and 7 ms.

Proton longitudinal relaxation times, T_1^H, were measured by the inversion-recovery method[19] and indirect detection via CP to the ^{13}C nuclei. Proton rotating frame relaxation times, $T_{1ρ}^H$'s, were also measured indirectly, using variable spin-locking times along with a fixed (usually 1 ms) CP time. T_1^H's and $T_{1ρ}^H$'s are found to be sensitive to the amount of water present; hence, in cases where meaningful comparisons of these parameters are made, samples were dried. Samples were dried in a vacuum at 140 °C unless otherwise indicated. For those samples where we were simply interested in extracting the CR line shape, it was advantageous to have some absorbed water in the sample because this shortened the intrinsic $T_{1ρ}^H$ of the NC regions and yielded a CR spectrum with a better signal-to-noise ratio.

At 7.05 T both ^{13}C and ^{1}H experiments were conducted. For CPMAS spectra, a 1-ms CP time was used; $ν_r$ = 6 kHz and radio frequency field strengths corresponded to 64 and 70 kHz nutation frequencies. During decoupling, TPPM modulation[20] was applied to the protons. Spectra of the CR and NC regions were isolated in the same manner as those at the lower field. Cylindrical, machined samples, 3 mm in diameter and 7−8 mm in length, were used.

For those experiments involving direct proton observation, a 5-mm CRAMPS (combined rotation and magic-angle spinning[21]) probe manufactured by Doty Scientific, Inc. was used. The radio frequency field strength corresponded to a 167-kHz nutation frequency (1.5 $μ$s 90° pulse). For acquisition of Bloch-decay signals, the probe dead time was 2 $μ$s and the dwell time was 1 $μ$s.

A proton multiple-pulse sequence[22] was used for measuring an average long period (the sum of CR plus NC thicknesses).

(16) *Dana's New Mineralogy*; Gaines, R. V., Skinner, H. C. W., Foord, E. E., Mason, B., Rosenzweig, A., Eds.; John Wiley and Sons: New York, 1997; pp 1480f.

(17) Schaefer, J.; Stejskal, E. O.; Buchdahl, R. *Macromolecules* **1977**, *10*, 384.

(18) VanderHart, D. L.; Pérez, E. *Macromolecules* **1986**, *19*, 1902.

(19) Farrar, T. C.; Becker, E. D. *Pulse and Fourier Transform NMR*; Academic Press: New York, 1971; pp 20f.

(20) Bennett, A. E.; Rienstra, C. M.; Auger, M.; Lakshmi, K. V.; Griffin, R. G. *J. Chem. Phys.* **1995**, *103*, 6951.

(21) Ryan, L. M.; Taylor, R. E.; Paff, A. J.; Gerstein, B. C. *J. Chem. Phys.* **1980**, *72*, 508.

In this spin diffusion[23] type of experiment, nonspinning samples are used and the preparation period involves application of the MREV-8[24,25] spin-locking sequence, during which individual protons relax according to their intrinsic rates, T_{1xz}.[26] (T_{1xz} relaxation is similar to $T_{1\rho}{}^H$ relaxation in the sense that the spectral density of motions, principally in the mid-kHz regime, is probed. The difference is that spin diffusion is suppressed in the T_{1xz} decay and is present in the $T_{1\rho}{}^H$ experiment; hence, $T_{1\rho}{}^H$ depends on an average spectral density over a region while T_{1xz} is sensitive to the spectral density for each proton.) In the preparation period which we set equal to 49 ms, T_{1xz}-type spin locking is sufficiently long so as to reduce the NC polarization to a level near zero while maintaining a finite polarization within the less mobile crystalline regions. The preparation period ends with the conversion of this spin-locked magnetization into Zeeman magnetization, which in turn, is made to alternate in sign upon successive scans. Following preparation, there is a variable spin diffusion time, t_{sd}, where polarization moves from the CR to the NC regions. Finally, there is another period of observed T_{1xz} decay with a spin-locking time of about 60 ms. The growth of the NC magnetization and the loss of the CR component is monitored as a function of t_{sd}. The decay profile corresponding to the CR component is extracted from the T_{1xz} decay at very short t_{sd}. The influence of $T_1{}^H$ relaxation during the spin diffusion time is corrected for by renormalizing each decay to the same initial amplitude.

Differential Scanning Calorimetry Measurements. DSC was performed on a TA Instruments DSC-10. The conditions for the first DSC run were as follows: heating rate of 10 °C/min (30 to 245 °C) and cooling rate of 1 °C/min (245 to 30 °C) in N_2. The conditions for the second run were as follows: heating rate of 10 °C/min (30 to 245 °C), and a cooling rate of 10 °C/min (245 to 30 °C) in N_2.

NnC Melt Blending. Unless otherwise indicated, extrusion of nylon-6 with the organically modified montmorillonite clays was performed in a Haake MPC/V-30 intermeshing co-rotating twin screw extruder (temperatures: 240 °C melting zone, 210 °C mixing zone, 245 °C die). Kneading blocks were situated at 75 and 187 mm.

Error estimates: Errors given for all quantities that we measured are standard error estimates unless otherwise indicated.

DSC Results

Representative DSC melting and crystallization curves for the pure nylon-6 and two of the nylon-6/clay NnC's are compared in Figure 1. We used annealed samples, N6-b, N6C-B-M1-c (blended NnC), N6C-Is-M-c, and N6C-Is-M-h (IsP NnC's). These latter samples differ in that N6C-Is-M-c has been injection molded at 295 °C and N6C-Is-M-h has been slow cooled from 253 °C prior to their common annealing histories. Some of the NMR measurements to be described indicated that the injection molded sample underwent irreversible changes; hence, we are interested in whether there are DSC differences that might shed light on the origin of these changes.

For the DSC measurements, two cycles of heating and cooling were applied. In the first cycle, samples were thermally ramped to 245 °C at 10 °C/min and then cooled to ambient temperature at 1 °C/min; the latter duplicates the SC protocol. Then, these SC samples were heated again to 245 °C at 10 °C/min and then cooled, this time at 10 °C/min. A perspective on this DSC data is that the crystallite form represented in these samples varies. NMR analysis (vide infra and Table 1) showed that for the NnC samples, both annealed and SC, the γ-form dominates (>85%) the crystallite population; the only exception is the annealed N6C-Is-M-c sample where the α-form comprises about two-thirds the crystalline fraction. The α-phase is exclusively present in the N6-b (pure nylon-6) sample.

The data shown in Figure 1 reveal several aspects of the melting and crystallization behavior for the three samples. For the annealed samples in Figure 1a, the blended NnC and the pure nylon-6 samples have very similar peak positions (222 °C) *even though the crystallites are of different forms*. (In the absence of clay, the γ-phase is reported[27] to have a melting point about 8 °C below that of the α-phase.) At the same time, there is a lower melting shoulder in the blended NnC, suggesting that a modest amount of crystallization takes place during cooldown from the annealing temperature. The higher peak positions, 225 °C for N6C-Is-M-h and 227 °C for N6C-Is-M-c, are surprising from the point of view that the N6C-Is-M-h sample is dominated by the γ-phase. The relative positions of these peaks are qualitatively consistent with the following notions: (a) the presence of the clay increases the peak melting point, (b) this temperature increment is higher for the IsP NnC compared to the blended NnC, *and* (c) for similar states, the α-crystallites melt at higher temperatures than their counterpart γ-crystallites. The latter point explains some of the difference between the IsP NnC's. Anticipating later discussions, we note that there is no significant low-temperature shoulder for sample N6C-Is-M-c that might suggest a degradation in molecular mass associated with the higher processing temperature. The higher melting temperatures of the two IsP samples, relative to the blended NnC, may be a consequence of many chain ends being covalently tethered to the organic modifier, which in turn, is ionically bonded to the clay surface. Tethering, which represents a stronger interaction with the surface than what would be expected in the blended NnC's, would reduce melt entropy, thereby raising the melting temperature. We will ignore, for the moment, the recrystallization data at the slower cooling rate for the annealed samples.

For the SC samples in Figure 1b the melting endotherms are broader and, as expected, appear at lower temperatures, relative to those of the annealed samples. The ordering of the peak melting temperatures, N6C-Is-M-h < N6C-B-M1-c < N6C-Is-M-c < N6-b, is completely different from the annealed samples. The SC history seems to accentuate the differences based on the higher melting α-crystallites. The reasons for the differences between NnC's, particularly between the IsP samples, are not understood. The typically broader low-temperature wings of the NnC endotherms might suggest that the clay produces some frustration of crystal-

(22) Havens, J. R.; VanderHart, D. L. *Macromolecules* **1985**, *18*, 1663.

(23) Abragam, A. *The Principles of Nuclear Magnetism*; Oxford University Press: London, 1961; Chapter V.

(24) Rhim, W.-K.; Elleman, D. D.; Vaughan, R. W. *J. Chem. Phys.* **1973**, *59*, 3740.

(25) Mansfield, P.; Orchard, J.; Stalker, D. C.; Richards, K. H. B. *Phys. Rev.* **1973**, *B7*, 90.

(26) Vega, A. J.; Vaughan, R. W. *J. Chem. Phys.* **1978**, *68*, 1958.

(27) Murthy, N. S.; Aharoni, S. M.; Szollosi, A. B. *J. Polym. Sci. Polym. Phys. Ed.* **1985**, *23*, 2549.
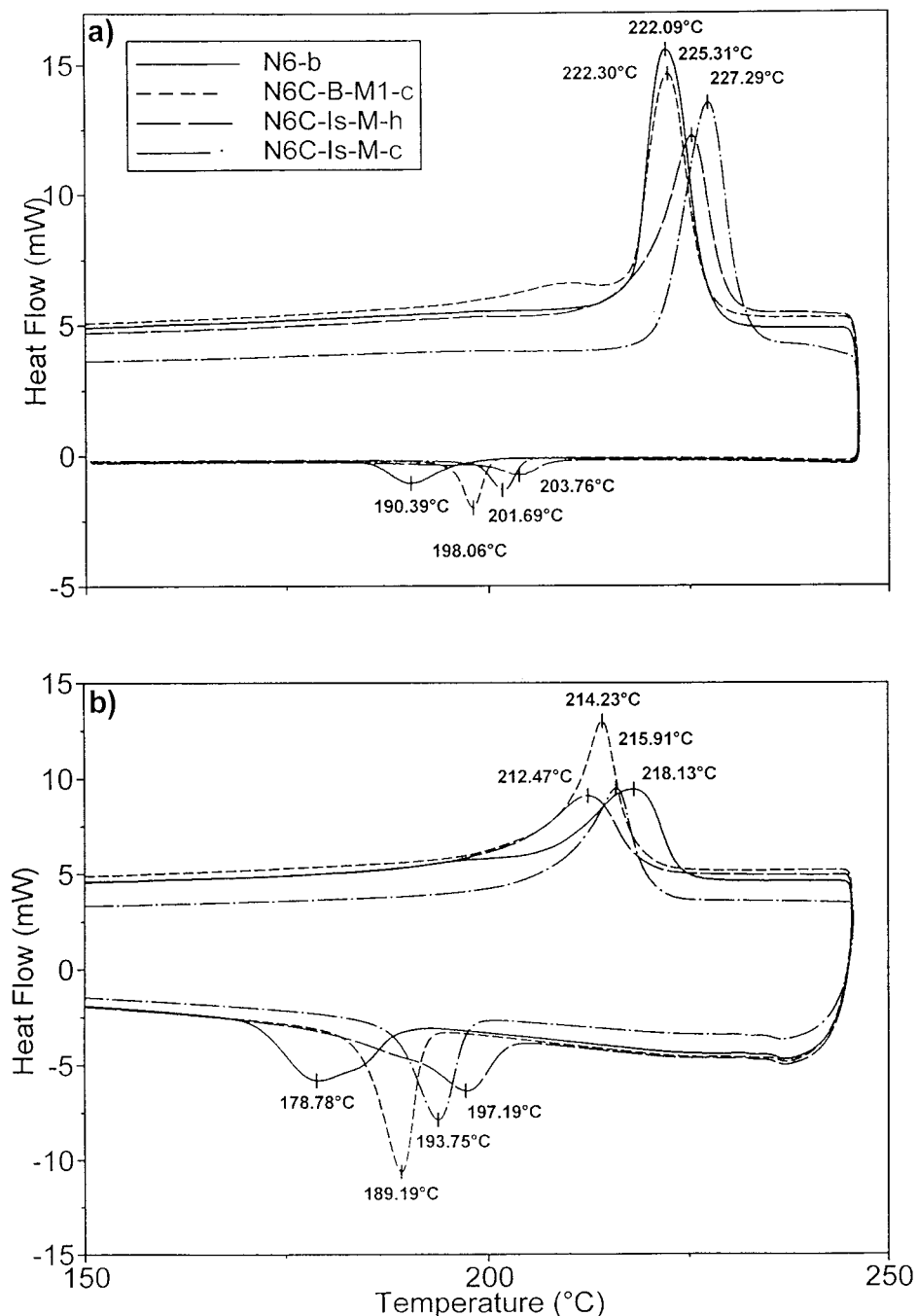
Figure 1. DSC thermograms for the indicated 214 °C annealed samples of nylon-6 plus three nanocomposites (NnC's). See Tables 1 and 3 for sample descriptions. (a) First runs: heating at 10 °C/min and cooling at 1 °C/min to simulate the slow cooling (SC) protocol used in this study. (b) Second runs on the cooled products of the first runs: both heating and cooling at 10 °C. Peak temperatures are indicated for both endo- and exotherms. Presence of clay clearly promotes nucleation at temperatures higher than that for nylon-6. For other deductions, see text.

lite size, leading to a larger fraction of thinner crystallites, compared with the N6 sample; however, that view is not supported by the NMR results.

The exothermic peak positions associated with the crystallization behavior of these samples varies from sample to sample; however, the relative ordering, N6C-Is-M-h > N6C-Is-M-c > N6C-B-M1-c > N6-b, is the same at both 1 and 10 °C/min cooling rates. The presence of the clay obviously facilitates nucleation of the crystallites because the peak for the blended NnC appears 8−10 °C higher and the peaks for the IsP NnC's appear 11−18 °C higher than the corresponding peak positions for pure nylon-6. Again, the higher increment

associated with the IsP NnC's, relative to the blended NnC, may arise from chemical tethering where chains attached to a surface at one end lose less entropy upon crystallization, compared to a free chain. If we follow this same line of reasoning, one hypothesis to explain why the peak position for N6C-Is-M-h is consistently higher than that for N6C-Is-M-c is that some of the points of attachment have broken during the 295 °C injection molding process. The narrower character of most of the NnC exotherms, compared to that of nylon-6, probably indicates that the number of nuclei formed at the clay surfaces is very high compared to pure nylon-6 and that crystal growth in any direction is
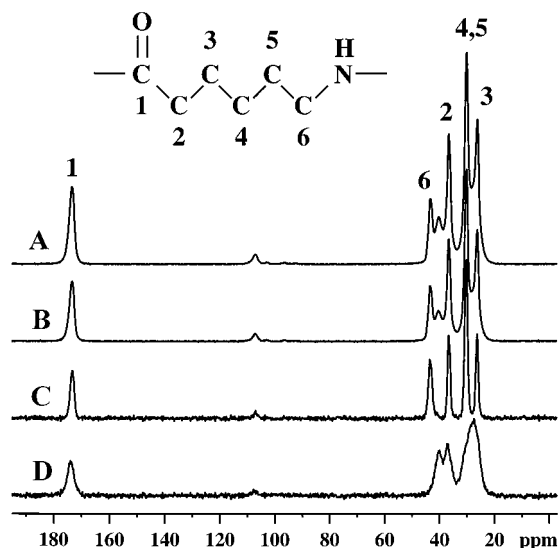
Figure 2. Illustration of the $T_{1\rho}{}^H$-based method for separating 75-MHz ^{13}C CPMAS spectra into contributions arising from the crystalline (CR) and the noncrystalline (NC) regions. The sample is pure nylon-6. Experimental spectra, A and B, respectively have 0- and 7-ms periods of proton spin locking prior to the 1-ms cross-polarization (CP) period. Spectrum A is relatively richer in the NC component compared to B because the intrinsic $T_{1\rho}{}^H$ for protons in the NC region is much shorter than for those in the CR region. Spectra C and D respectively represent the CPMAS spectra of the CR and the NC regions; these spectra are different linear combinations of A and B, chosen to segregate the "CR" component (α-form here) with the narrower line widths from the "NC" component with the broader line widths. Apparent NMR crystallinities are determined from the relative integrals of the CR and NC contributions whose sum is spectrum A. Corrected values of the crystallinities, f_c, appearing in Table 1 are based on measured differential amounts of $T_{1\rho}{}^H$ decay during the 1-ms period of CP pertaining to spectrum A. The structure of nylon-6 is also shown along with the spectral assignments of the "CR" resonances according to ref 25.

much more restricted (both in space and time) than in nylon-6.

NMR Results

Separation of Signals from Crystalline Domains and Allomorph Identification. Because many of our observations pertain to the crystalline phase of the nylon-6, we first illustrate the separation of NMR signals into those of the crystalline (CR) and the noncrystalline (NC) regions. This separation[18] is based on differences in the intrinsic rotating-frame relaxation time, $T_{1\rho}{}^H$, that characterize the CR and the NC regions. This separation method has been modeled mathematically[28] for an ideal, two-phase system and has been shown to give a slightly distorted separation of the CR and the NC signals because of the phenomenon of proton spin diffusion. However, in the case we are considering, these distortions are not expected to alter in any significant way the arguments we present. In Figure 2 we illustrate, for the N6 sample, the separation of 75-MHz ^{13}C signals into their CR and NC contributions for the N6 sample. Spectra 2A and 2B correspond, respectively, to 0- and 7-ms proton spin-locking times

prior to the 1-ms cross-polarization (CP) time. During these spin-locking times, the proton polarization decays faster in the NC regions than in the CR regions. Hence, the intensity contribution from the CR regions is relatively greater in spectrum 2B. Spectra 2C and 2D are linear combinations of spectra 2A and 2B where we have attempted to null the NC and CR signal contributions, respectively. The linear combinations that are chosen to represent the CR and the NC contributions are based on the notions that the order is higher and the molecular mobility is lower in the CR region; both of these factors translate into typically narrower intrinsic line widths for those carbons found in CR regions compared with corresponding carbons occupying NC positions. Consistent with this notion, line widths are considerably narrower in spectrum 2C than in 2D. According to other studies,[29] the crystalline form of this nylon-6 is the α-form. The peak assignments previously made,[29,30] along with the structure of the nylon-6 repeat unit, are also given in Figure 2.

Figure 3 illustrates a few points about the crystal allomorphs typical of both nylon-6 and these NnC's and about the dependence of the CR line shape on the static magnetic field. In Figures 3A and 3B, we respectively show 25-MHz CR spectra (aliphatic region only) for samples N6C-B-L1-a (as received) and N6C-B-L1-b ("slowly cooled" at 1 °C/min). These spectra are contrasted with the N6 spectrum of pure SC nylon-6 (Figure 3C). Counterpart 75-MHz spectra corresponding to spectra 3B and 3C are given in 3D and 3E, respectively. In comparing spectra 3B and 3C with 3D and 3E, one notes that there is a dramatic improvement in resolution at 75 MHz, relative to 25 MHz, mainly on the downfield side of the spectra. This change in line width and line shape is a well-understood phenomenon[31] associated with dipolar couplings between ^{13}C nuclei and a quadrupolar ^{14}N nucleus that experiences a non-zero electric field gradient. The ^{13}C resonances most strongly affected are those closest to the amide nitrogen including the carbonyl resonance (not shown). Spectrum 3B shows no intensity at 26.3 ppm; hence, there is no significant α-content in the CR regions in this slowly cooled NnC sample. The resonances of Figures 3B and 3D are entirely consistent with those reported[29] for the γ-form of crystalline nylon-6. Note that a unique resonance of the γ-form, identifiable at both fields, is the resonance at 34 ppm, while the peak at 26.3 ppm is a convenient indicator of the α-form. Hence, using these two resonances at either field, it is possible to assay the a/γ ratio in samples where both forms are present. Tabulation of f_α, that is, that portion of the CR material which is in the α-form, is given in Table 1. Spectrum 3A illustrates a case where both α- and γ-crystallites coexist, as evidenced by resonances at both 26.3 and 34 ppm.

The other slowly cooled nylon-6/clay NnC's, N6C-B-M1-b, N6C-B-M2-b, and N6C-Is-M-f, gave spectra (not shown) nearly identical to those of spectrum 3B and 3D

(28) VanderHart, D. L.; Alamo, R. A.; Nyden, M. R.; Kim, M.-H.; Mandelkern, L. *Macromolecules* **2000**, *33*, 6078.

(29) Hatfield, G. R.; Glans, J. H.; Hammond, W. B. *Macromolecules* **1990**, *23*, 1654.

(30) Okada, A.; Kawasumi, M.; Tajima, I.; Kurauchi, T.; Kamigaito, O. *J. Appl. Polym. Sci.* **1989**, *37*, 1363.

(31) Zumbulyadis, N.; Henrichs, P. M.; Young, R. H. *J. Chem. Phys.* **1981**, *75*, 1603. Hexem, J. G.; Frey, M. H.; Opella, S. J. *J. Chem. Phys.* **1982**, *77*, 3847.
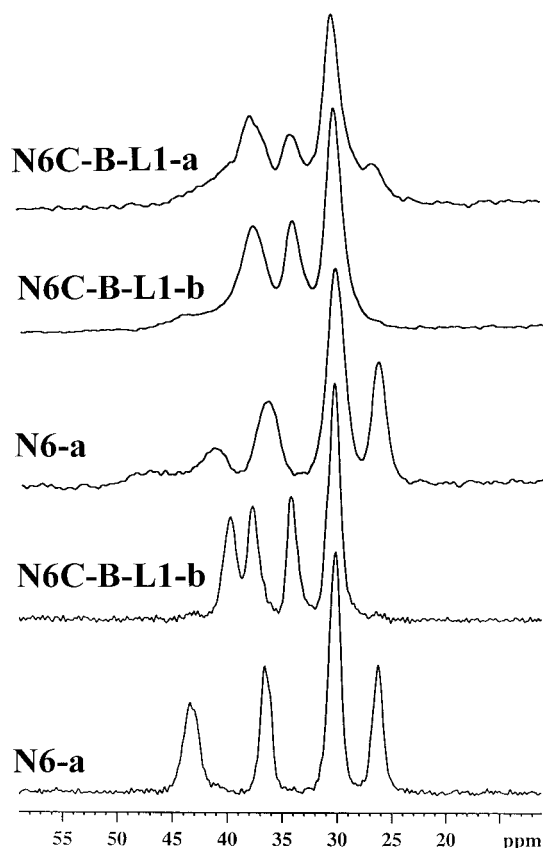
Figure 3. Comparison of the aliphatic regions of the "CR" spectra of the indicated nylon-6 and NnC samples. Spectral differences traceable to the presence of clay, to crystallization conditions, and to the static field are illustrated. The upper three spectra have been taken at 25 MHz and the lower two at 75 MHz. Note the dominance of the α-form for nylon-6 (N6-a) and the γ-form in the spectra of the NnC's; this latter dominance increases by decreasing the cooling rate during crystallization (upper two spectra). Note also the sharpening of resonances at 75 MHz compared with 25 MHz; this is especially true for the most downfield resonances associated with C6, which is bonded to the amide ^{14}N quadrupolar nucleus. The 26.3 ppm resonance of the α-form and the 34.0 ppm resonance of the γ-form are unique resonances that allow one to evaluate the α/γ ratio at either field.

(see Table 1). That is to say, when cooled from the melt at 1 °C/min, the nylon, in the presence of nanodispersed clay, melt-crystallizes almost exclusively into the γ-form. This is true for both IsP and blended NnC's. In contrast, the presumed faster cooling of the as-received NnC's, including N6C-B-M1-a and N6C-B-M2-a, produced minor fractions of the α-form along with a slightly lower crystallinity (Table 1). From the foregoing, it is clear that the different mixtures of crystal forms present in the same material is, to some extent, a function of thermal history. The dominance of the γ-form for these nylon-6/clay composites is consistent with the findings of others;[32,33] namely, that in contrast to pure nylon where the α-form is exclusively found under a wide range of crystallization conditions, the presence of exfoliated, nanodispersed clay in the nylon-6 strongly promotes the development of γ-form crystallites. On this

(32) Kojima, Y.; Usuki, A.; Kawasumi, M.; Okada, A.; Kurauchi, T.; Kamigaito, O.; Kaji, K. *J. Polym. Sci. (B) Polym. Phys.* **1994**, *32*, 625.

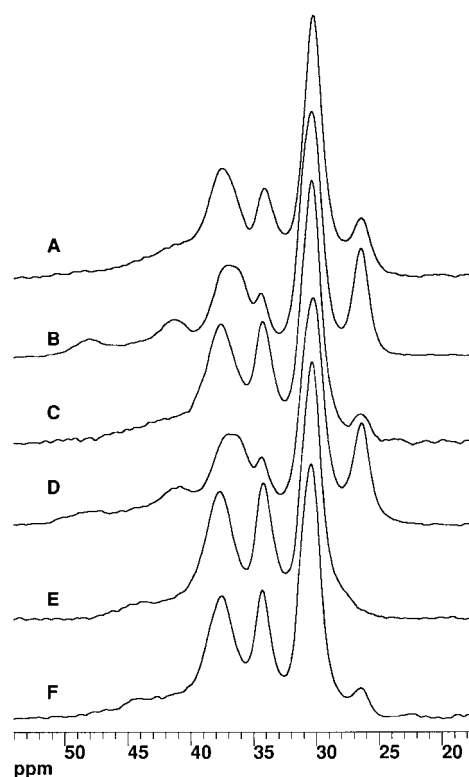(33) Maxfield, M.; Christiani, R.; Murthy, S. N.; Tuller, H. U.S. Patent 5,385,776, 1995.

Figure 4. Pairs of 25-MHz "CR" spectra, sequentially unannealed and annealed (214 °C) for three different preparations of the in situ polymerized (IsP) NnC. A and B: injection-molded at 295 °C [N6C-Is-M-(a,c) in Table 1]. C and D: injection-molded, remelted at 248 °C, and SC [N6C-Is-M-(d,e)]. E and F: SC from 253 °C [N6C-Is-M-(f,h)]. The processing history of injection molding at 295 °C creates an irreversible change leading to a higher fraction of α-form crystallites. This difference is more modest before annealing (spectra C and E) compared to after annealing (spectra D and F). Values of f_α for spectra A and B are respectively 0.34 ± 0.03 and 0.67 ± 005 but f_α values varied considerably for these injection-molded samples (see Table 1).

basis, one might be tempted to interpret the measured fraction of α-form crystallites in any given NnC in terms of the *inhomogeneity* of the distribution of the exfoliated clay within the nylon-6/clay NnC. Figure 3 suggests that if such an approach is to be successful, at the very least, a uniform thermal history must be adopted before spectral assessments of this inhomogeneity will be meaningful. We will address the issue of which experimental parameter is most reliably correlated with the homogeneity of clay dispersion in the second paper in this series.

Figure 4 illustrates variations in the α/γ ratio for the in situ polymerized (IsP) NnC, N6C-Is-M, whose material was also exposed to the most diverse set of preparatory histories. Given that, in crystallization from the melt, the production of the γ-form is promoted by the presence of the clay, it is also found by some[33] but not by others[9] that subsequent annealing in the vicinity of 200 °C tends to convert some portion of the γ-phase crystallites into α-phase crystallites. In Figure 4 we show the 25-MHz CR spectra of six of these NnC samples. Spectra 4A (one of the "a" samples in Table 1: injection molded at 295 °C), 4C (sample "d"= another portion of sample "a" subsequently remelted at 253 °C and slowly cooled at 1 °C/min), and 4E (sample "f": the original resin, compacted in a vacuum at 240 °C and

then remelted under nitrogen at 253 °C followed by slow cooling at 1 °C/min) correspond to samples prior to annealing. Spectra 4B, 4D, and 4F correspond to their respective counterpart samples, labeled "c", "e", and "h" in Table 1, which have been annealed for 18 h at 214 °C followed by relatively rapid air-cooling on the bench.

We note a few things about Figure 4. First, in comparing 4A with 4C, slow cooling from the melt produces a lower fraction of α-form crystallites, 0.10 ± 0.03, than does injection molding, 0.34 ± 0.04, where in the latter case, the rate of cooling is faster because the mold is initially at a temperature (85 °C) substantially below the melt temperature. However, annealing both of these samples at 214 °C for 18 h leaves materials with comparable α-form fractions (see Table 1) of 0.63 ± 0.05 and 0.67 ± 0.05, respectively. In contrast to this behavior are spectra 4E and 4F where limiting the temperature of the melted NnC resin to 253 °C results in pure γ-crystallites after slow cooling; moreover, upon annealing at 214 °C for 18 h, <12% of the crystalline material is converted to the α-phase. *Therefore, exposure at 295 °C along with the shear-flow stresses of the injection process have irreversibly changed something so that the γ-form crystallites become less dominant upon annealing at 214 °C.*

It was later in our study that we recognized large-scale *heterogeneity* of the injection-molded sample. This sample was injection molded as a thick disk, 7.3 cm in diameter and 0.85 cm in thickness; the injection port was radially centered. It was found that the percentage of crystallites of the α-form, before annealing, ranged widely from 0.10 to 0.47 over the 10 cylindrical samples (five samples were 6-mm o.d. and 12-mm long and five were 3-mm o.d. and 7-mm long), which were eventually machined from this disk, while the range after annealing these samples was 0.42–0.70. The increase in this fraction upon annealing was quite constant and in the 0.20–0.30 range. We also found that an unannealed sample that had absorbed some water during storage in the laboratory would experience an increase of about 0.05 in the fraction of α-form crystallites when dried at 135 °C in a vacuum. (We do not know whether this is strictly a thermal effect or whether the presence of water in conjunction with the drying temperature of 135 °C facilitates this transformation.) These 10 samples were taken from the center, middle, and edges of the disk as well as from the upper and lower surfaces; however, we failed to identify any correlation between position and the percentage of α-form crystallites; one could obtain wide variations in this percentage from cylinders machined from adjacent areas. Thus, the statement at the end of the foregoing paragraph stands; however, the supporting numbers, related to the α content before and after annealing, vary widely.

We could think of two hypotheses to explain this large, localized variation in the α content throughout this injection molded disk. First, this variation could reflect differences in cooling history, thereby suggesting a rather turbulent and radially uneven flow as the mold is filled by the injected molten NnC. A second possibility is that the clay concentration is very nonuniform on a large spatial scale, possibly because of poor initial mixing or, more interestingly, because this might be the result of the flow fields in the injection molding process.
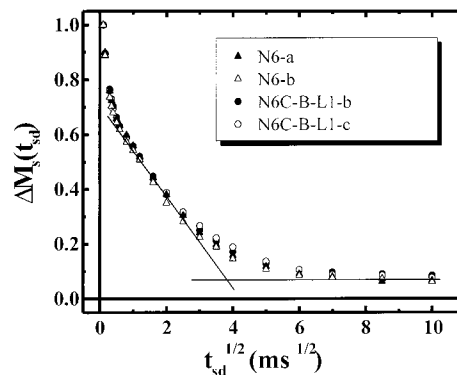

Figure 5. Relative amplitude changes, compensated for T_1^H relaxation, for the longer relaxing T_{1xz} components of the indicated samples in a spin diffusion experiment where the initial condition is established by a 49-ms T_{1xz} decay that generates a crystalline-rich polarization distribution. As spin diffusion time, t_{sd}, lengthens, polarization moves from the CR protons to the NC protons until the two regions are equilibrated (represented by $\Delta M_s(t_{sd}) = 0$ in this plot). The initial fast decay indicates that the NC polarization is not totally suppressed in the initial preparation, implying that the mobility throughout the NC region is not uniform, probably because H-bonding can create pockets of reduced NC mobility. The intersection of the drawn lines that define the slope and the longer time asymptote gives a $t_{sd}*$, which is used to establish a long period. The main deduction is that this long period is very constant, independent of the presence or absence of clay (a diamagnetic Laponite in this case) and independent of whether one anneals or does not anneal a SC sample.

In the second paper in this series, we will return, briefly, to these samples in connection with the presentation of T_1^H results because we will argue that T_1^H measurements, under the right circumstances, can be used to assay the quality (or reproducibility) of clay dispersion. As a preview, those T_1^H results indicated only minor variations in clay dispersion. Thus, we ultimately concluded that *differences in cooling history lead to the large observed variation in the α-phase fraction across the injection-molded disc.* To the extent that the mechanical properties of the α- and γ-crystallites are different, mechanical properties may then show exaggerated dependences on cooling history.

Crystallite Thickness and Long Period. The spin diffusion experiment, described earlier at the end of the "NMR Spectroscopy" section and based on a T_{1xz} preparation and readout, was used to obtain a measure of the "long period" (the sum of the average crystallite thickness plus the noncrystalline domain thickness). Data, plotted as a function of the square root of spin diffusion time, are shown in Figure 5 for nonspinning samples N6 and N6C-B-L1, both before and after annealing. Given the influence of the paramagnetic montmorillonite on $T_{1\rho}^H$ (to be discussed shortly), we wanted T_{1xz} to reflect only contributions from molecular mobility; hence, NnC's having only diamagnetic clay were chosen for this part of the study. We wanted this experiment to report spin diffusion only between the CR and the NC regions. In the preparation stage, polarization remains mainly in the CR region, having been prepared *in the absence of spin diffusion.* Thus, the initial spatial gradient of magnetization is expected to be strong at the CR/NC interface, thereby simplifying the mathematics for modeling spin diffusion. The ordinate in Figure 5 is a relative measure of the loss of CR

polarization, by spin diffusion, to the NC regions. An ordinate value of 0.0 represents polarization equilibrium between the protons in the CR and NC regions. The rapid initial drop in polarization is a sign that not all the initially prepared magnetization is in the CR region; that is, there are some protons in the NC region, perhaps those closest to NC hydrogen-bonding sites, whose mobility is restricted and whose intrinsic T_{1xz} is longer than the typical T_{1xz} of the NC region. After the preparation, polarization from these scattered, less-mobile NC protons moves quickly to the neighboring NC protons whose T_{1xz}'s are much shorter. After a spin diffusion time of 0.5−1 ms, such intraphase polarization gradients should equilibrate.[34] Hence, a conservative approach is to regard the data beyond $t_{sd} = 1$ ms to be defined entirely by interphase spin diffusion between the protons in CR and NC domains. By extending the initial slope of the plots of Figure 5 from a time of about 1 ms onward, one finds that these slopes all intersect the abscissa near $(t_{sd}*)^{1/2} = 3.9$ ms$^{1/2}$. Translating[35,36] this $t_{sd}*$ into a long spacing, L, for the case of a lamellar morphology, a crystallinity of 0.40 (see Table 1) and a diffusion constant, D, for both CR and NC regions of 0.7 nm²/ms[35] gives a long spacing of 15.3 nm and a crystallite thickness of 6.1 nm. The relevant equation is

$$L = 2(f_c f_{nc})^{-1}(Dt_{sd}*/\pi)^{1/2} \qquad (1)$$

where f_c and f_{nc} are respectively the mass fractions of the CR and the NC regions. *Similar behavior for all four samples in Figure 5 means that the long period does not change appreciably, relative to the long period of pure nylon-6, by either annealing at 214 °C or by the introduction of the (Laponite) clay.* The initial slope is more sensitive to a change in the long period than it is to a change in f_c owing to the slow change in the term $(f_c f_{nc})$ for typical f_c values near 0.40−0.45 (see Table 1).

Expected Influence of Montmorillonite Fe³⁺ on Proton Longitudinal Relaxation Times, T_1^H. Most clays are thin (1.0−1.5 nm) platelike, naturally occurring aluminosilicates with mainly silicate tetrahedra at the surfaces and with octahedral sites, containing aluminum, in the midplane of the layers. Montmorillonite clays vary considerably in composition; average compositions[16] show about 17% of the octahedral Al³⁺ sites occupied by Mg²⁺ and perhaps 4% of the tetrahedral silicon sites occupied by Al³⁺. These substitutions result in embedded negative charges at these sites of substitution. This negative charge requires neutralization, usually with a cation that is located at the surface of the clay layer. When one wishes to mix a clay with a polymer, one typically introduces a so-called organic modifier (OM), which is used to compatibilize the clay surface with the polymer. The OM is usually an organic cation and is often a substituted ammonium ion. These bulkier cations displace the normal inorganic cations found in clay and they form ionic bonds at the sites of the embedded negative charges in the clay. The effectiveness of the organic modifier in promoting mixing between polymer and clay is, in part, a result of

improving the enthalpic and entropic aspects of the thermodynamics of mixing and, in part, a weakening of the clay−clay interactions (by forcing the gallery spacing between clay layers to be larger than when the inorganic cations were present).

Less numerous paramagnetic Fe³⁺ ions also substitute into the octahedral Al³⁺ sites. The presence of the Fe³⁺ ions has no influence on the embedded charge; however, these ions are strongly paramagnetic ($S = {}^5/_2$ in this distorted octahedral environment[37]) and can exert a sizable influence on the nuclear spins near the clay surface. An excellent article has appeared[8] describing the impact of Fe³⁺ ions on Li⁺ spins in **intercalated** montmorillonite clays. We will refer to that work as we outline the role that the Fe³⁺ ions are expected to play in our exfoliated system.

The density of Fe³⁺ atoms in the montmorillonites varies according to the natural source. According to elemental-analysis information from Southern Clay Products, we compute that there is one Fe³⁺ substitution for every 10.2 octahedral sites in all the montmorillonite clays obtained from them. This translates into a mean area per Fe³⁺ atom of 1.16 nm²; hence, we deduce an average Fe−Fe distance of 1.08 nm. This average, however, only controls the statistics of Fe³⁺ substitution because the lattice defines the discrete possible distances between octahedral sites. We also do not know the deviations in Fe³⁺ content that exist from batch to batch in this montmorillonite clay. Also, while it is believed[16] that in montmorillonite the Fe mainly resides in the octahedral sites, some substitution into the tetrahedral sites is, in principle, possible. Finally, there are indications[38] in some montmorillonite clays that Fe exists in Fe-rich regions outside of the clay layers. No attempt has been made to explore these possibilities. Hence, while we believe that what we report will be applicable to other montmorillonite clays with similar Fe contents, we cannot be sure. The density of Fe³⁺ in the IsP NnC's from UBE was not available; however, as we shall see, the effective average density is certainly lower than that of the Southern Clay materials.

Because a clay layer is only about 1-nm thick and because the Fe³⁺ ions are at the midplane of the layer, the protons of the organic modifier on the clay can become as close as 0.5−0.6 nm from the Fe³⁺ ions; such protons, as well as certain nylon-6 protons that are very proximate to the surface, will experience both a direct line broadening and a shortening of T_1^H. A proton at a distance of more than 0.5 nm from an Fe³⁺ ion will, to a good approximation, see all five unpaired electrons as being localized at the Fe³⁺ nucleus. In this sense, electron−electron spin exchange events among the five electrons on a given Fe³⁺ atom will not produce any significant fluctuation of the proton local field because spin exchange preserves the net electron moment. However, at a particular proton site, electron−electron spin-exchange events[39] between electrons on *different* Fe³⁺ atoms will cause a local field fluctuation owing to the high probability that the proton in question will not

(34) VanderHart, D. L. *Macromolecules* **1994**, *27*, 2837.

(35) Clauss, J.; Schmidt-Rohr, K.; Spiess, H. W. *Acta Polym.* **1993**, *1*, 44.

(36) VanderHart, D. L.; McFadden, G. B. *Solid State Nucl. Magn. Reson.* **1996**, *7*, 45.

(37) Bensimon, Y.; Deroide, B.; Zanchetta, J. V. *J. Phys. Chem. Solids* **1999**, *60*, 813.

(38) Goodman, B. A. *Clay Miner.* **1978**, *13*, 351.

(39) Poole, C. P. *Electron Spin Resonance*; Interscience Publishers: New York, 1967.

have equal dipolar couplings to the two exchanging Fe^{3+} sites. The quantity, "τ_e", as we will use the term, is, for any process, including both intersite electron spin exchange and the electron spin−lattice relaxation time, T_1^e, the characteristic time over which a fluctuation occurs in the net electron moment of a given Fe^{3+} ion. When the average distance between Fe^{3+} atoms is near 1 nm, as is true for the Southern Clay NnC's, it is expected[8] that, at ambient temperature, spin exchange between electrons on different atoms will happen on a time scale of about (10^{-9} s), that is, close to the Larmor period of the protons. If that expectation is correct, then an important influence on the protons will be a shortening of T_1^H where, for a given Fe^{3+} atom and a given nearby proton, the direct paramagnetic contribution to its intrinsic T_1^H will be proportional to the sixth power of the electron−nuclear distance.[40] There will also be some line broadening; however, line broadening will, by no means, be as severe as it would be if τ_e were, say, $>10^{-5}$ s, that is, greater than the inverse of the dipolar interaction between the electron and the nucleus. In the latter case, serious loss of signal would also ensue. As will be seen presently, significant electron−nuclear dipolar line broadening exists and its origin is, in part, fluctuational (as just discussed) and, in part, static. The static component arises from the persistent, non-zero, thermally averaged polarization of each electron spin. That polarization is, at 7.05 and 2.35 T, respectively about 1.6 and 0.53% of the maximum theoretical electron polarization. Note that the magnitude of this static interaction is proportional to the applied static field, B_o. Note also that magic-angle spinning (MAS) should, in principle, be able to average this static component to zero over a rotor cycle. Establishing a mean electron polarization by thermal averaging over spin states is, however, not a particularly efficient or precise type of averaging, especially when the static averages are relatively small compared to the size of the fluctuations. Hence, we anticipate that MAS will only be partially effective in averaging to zero these quasi-static electron−nuclear dipolar interactions.

Because of rather efficient proton spin diffusion in nylon-6, the shortening of T_1^H will propagate well beyond those protons that are relaxed directly by the fluctuating local dipolar fields of the unpaired electrons. We will consider the impact of this local paramagnetic relaxation on more distant polymer spins in the second paper in this series.

Experimental Influence of Clay Paramagnetism on the Spectra of the Organic Modifier in the Absence of Nylon-6. To provide some experimental input into the influence of the iron paramagnetism on the NMR observables, we examined the two organically modified clays (OMCs) that were used in fabricating NnC's N6C-B-M1 and N6C-B-L1. The OM, MT(HE)$_2$AI (= methyl, hydrogenated-tallow, bis-2-hydroxyethyl, quaternary ammonium ion made by exchanging the clay with the corresponding ammonium chloride at 0.95 equiv/kg of clay), was identical in these two materials. The clays themselves differed in that the montmorillonite is paramagnetic and the Laponite, a synthetic magnesium silicate that contains no iron, is diamag-
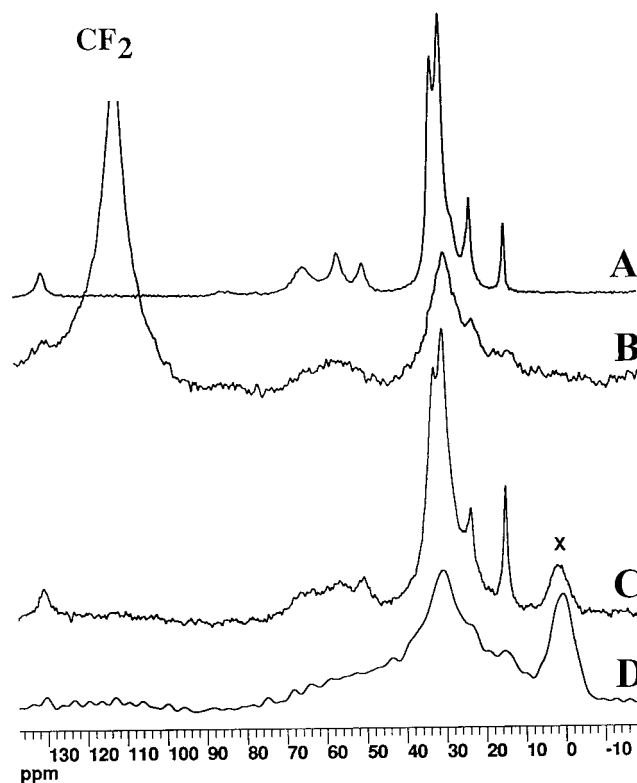
(40) Blumberg, W. E. *Phys. Rev.* **1960**, *119*, 79.

Figure 6. Illustration of the influence of clay paramagnetism (versus diamagnetism) on the ^{13}C spectra of nuclei within 0.4 nm of a clay surface. Spectra of the organic modifier (OM), methyl, tallow, bis-2-hydroxyethyl, quaternary ammonium ion, at 25 and 75 MHz for organically modified clays (OMCs) containing diamagnetic Laponite versus paramagnetic montmorillonite (mmt) clays. A: Laponite, 75-MHz CPMAS (1-ms CP time), ν_r = 5 kHz. B: Mmt, 75 MHz, ν_r = 5 kHz. C: Laponite, 25 MHz, ν_r = 4 kHz. D: Mmt, 25 MHz, ν_r = 4 kHz. In these samples, the OM is about 30% of the total mass of the OMC. Considering the gallery spacing and the average density of Fe^{3+} ions in the clay layers, for this mmt OMC most nearest-neighbor C−Fe distances should be in the range from 0.6 to 1.1 nm with some distances possibly being higher, depending on the randomness of the distribution. These are Bloch-decay spectra except for spectrum A; Bloch-decay spectra are slightly more quantitative than CPMAS spectra for the Laponite OMC and much more quantitative for the mmt OMC. However, in these mmt OMC spectra the paramagnetic influence is not even fully represented because there is also substantial signal loss (see text), presumably because many of the resonances are broadened beyond observability. Note that the subset of observable resonances in the mmt OMC spectra are similarly broadened (in ppm) at both fields. There are interfering resonances near 0 ppm from a stator O-ring at 25 MHz (marked with an "X") and near 115 ppm (labeled CF$_2$) from tetrafluoroethylene spacers at 75 MHz.

netic. A qualitative comparison of the NMR characteristics of these samples should indicate the influence of Fe^{3+} on nuclei within about 0.4 nm of a clay surface because the layer spacing measured by X-ray scattering is about 1.8 nm (0.8 nm between adjacent clay surfaces) in both these materials.

Figure 6 compares the 25-MHz ^{13}C Bloch-decay (single-pulse excitation; 3-s repetition time) spectra obtained from the Laponite (6A) and montmorillonite (6B) OMCs. Included in Figure 6 are 75-MHz spectra of the Laponite OMC (6C = CPMAS) and the montmorillonite (6D = Bloch decay) OMC. The Laponite OMC spectra both have decent resolution, albeit the resolution

is slightly better at 75 MHz. In terms of assignments, the resonances below 40 ppm are associated with the hydrogenated tallow moiety. Hydrogenated tallow refers to mixed-length (usually including C12, C14, C16, and C18 components with an average length near C17[41]) linear aliphatic chains having animal origin whose unsaturated bonds (averaging about 0.5 bonds per chain before hydrogenation[41]) have been largely converted to saturated bonds. Resonances can be identified for the methyl carbon (14.7 ppm), the adjacent methylene (23.4 ppm), and the interior methylenes (30−33 ppm). The latter carbons that are in dynamic trans−gauche isomerization[42,43] give a peak at 30.4 ppm while those at 32.6 ppm are believed[43,44] to be somewhat more ordered, having average conformations closer to trans, even though they are by no means rigid as evidenced by ^{13}C longitudinal relaxation times, T_1^C, that are well below 1 s. The 45−70 ppm spectral region contains all the carbons bonded to the nitrogen plus the CH_2OH carbon of the hydroxy-ethyl groups.

In contrast to the good spectral resolution of the Laponite OMC, the montmorillonite OMC spectra in Figure 6 have significantly worse resolution, although there is a slight improvement in resolution at 75 MHz vs 25 MHz. At 25 MHz, the spectrum of the montmorillonite OMC can be approximately matched by applying a 250-Hz line broadening to the spectrum of the Laponite OMC. However, an important difference between the spectra of the Laponite and montmorillonite OMCs is that the relative Bloch-decay intensity per scan for equal amounts of material is, for the montmorillonite sample, about one-third (25 MHz) and about one-fourth (75 MHz) that of the Laponite sample. (According to the stoichiometries used in preparing these two OMCs, the Laponite should have about 5% more OM than the montmorillonite; hence, the loss of signal cited is close to that based on equivalent amounts of the OM.) The larger loss at the higher field is qualitatively consistent with the fact that the thermally averaged electron moments are larger. We were at first surprised that in the 75-MHz spectra of the montmorillonite OMC relative to the Laponite OMC, there was only about a 20% greater loss of relative intensity for the 45−70 ppm region relative to the 15−40 ppm spectral region. We expected the carbons associated with the former region to be, on average, closer to the clay surface. However, it has previously been recognized[8] that when multiple layers are so close, Fe sites in both bracketing clay layers typically contribute to the dipolar fields at a given OM nucleus. Then, that summed dipolar field strength becomes much less sensitive than the inverse cube of the distance to either of the clay mid-planes. Therefore, a qualitative conclusion, in view of the significant overall signal loss, is that *the observed ^{13}C signals more strongly reflect statistical variations in local Fe concentration within a pair of layers rather than variations in distance from the clay mid-planes.* This bias for selected ^{13}C signals should be kept in mind as we summarize other measurements associated with these OMCs.

(41) *Analysis and Characterization of Oils, Fats and Fat Products*; Boekenoogen, H. A., Ed.; Interscience Publishers: London, 1968; Vol. II, p 290.
(42) Randall, J. C.; Hsieh, E. T. *ACS Symp. Ser.* **1984**, *247*, 131.
(43) Earl, W. L.; VanderHart, D. L. *Macromolecules* **1979**, *12*, 762.
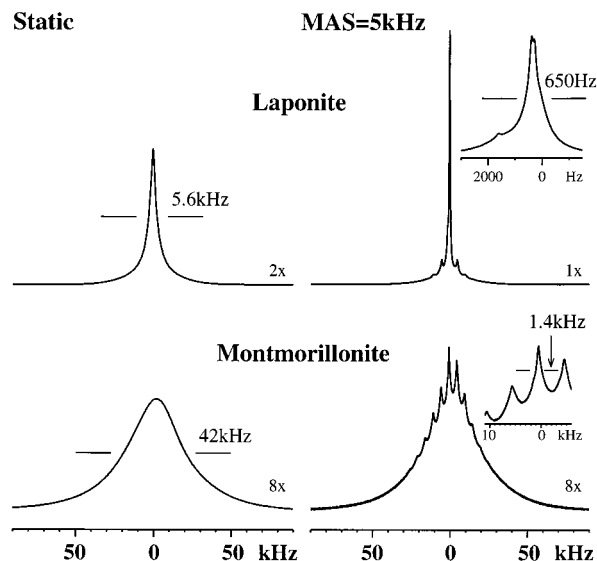(44) Tonelli, A. E. *Macromolecules* **1978**, *11*, 565 and 634.

Figure 7. 300-MHz proton Bloch-decay spectra of diamagnetic Laponite and paramagnetic mmt OMCs showing the corresponding line shape changes for nonspinning (left side) and ν_r = 5 kHz (right side). Vertical scaling factors from a reference state having equal total intensities are also shown. The paramagnetism of the mmt clay produces about a 30-kHz broadening of the broader Laponite components. The ability of MAS to average out the electron−proton dipolar interactions (expected only when the electrons can be replaced by highly thermally averaged electrons) is poor (only about 15% of the total intensity is in the narrowed centerbands plus sidebands) when the dipolar fluctuations are very large compared to the thermal averages and the correlation time for the fluctuations is of the order of 10^{-9} s. We speculate that the spinning sidebands in the mmt spectrum mainly arise from those locations where, statistically, the electron−proton dipolar interactions are weaker.

Using different spin-locking times and a 1-ms CP time, the approximate proton rotating frame relaxation time, $T_{1\rho}^H$, at 100 MHz is indirectly measured to be 3.0 ± 0.5 ms for the OMC protons in Laponite. This $T_{1\rho}^H$ indicates some degree of molecular motion but, by itself, is not a precise gauge of the amplitudes and correlation times for this motion. A similar indirect $T_{1\rho}^H$ measurement for the protons of the montmorillonite OMC failed owing to its very short $T_{1\rho}^H$. An estimate of $T_{1\rho}^H = 150 \pm 50$ μs was finally obtained using a CP time of 0.1 ms. This $T_{1\rho}^H$ reflects additional biases favoring sites of least mid-kHz spectral density of molecular motions, fastest cross polarization, and lowest local Fe^{3+} concentration.

We also observed protons directly, but only at 7.05 T (300-MHz proton frequency). We briefly summarize our findings for the two OMCs with the Laponite values listed first and the montmorillonite values in parentheses. (A) T_1^H's are 164 ms (4.7 ms), so the paramagnetic Fe^{3+} ions exert a strong influence on T_1^H. (B) Total intensity per scan-mg in a proton Bloch-decay spectrum with a 1.5-ms 90° pulse excitation is 1.00 (0.64). Thus, even a strong proton pulse with a wide receiver bandwidth is only able to recover about two-thirds of the total signal. (C) As illustrated in Figure 7, for the Bloch-decay proton signal of the montmorillonite clay and ν_r = 5 kHz, about 10−15% of the intensity can be identified as "narrower centerband plus associated sidebands". Hence, MAS is capable of producing a modest amount of line narrowing. In addition, for a nonspinning sample,

an exponential line broadening of $\gg 30$ kHz applied to the Laponite signal creates a good match **to the broader components of the montmorillonite signal.** (Recall that $200-250$ Hz of line broadening at a MAS frequency of 4 kHz, when applied to the observed ^{13}C Laponite signal, gave approximate agreement with the ^{13}C montmorillonite Bloch-decay signal at 2.35 T. The need for this larger 30-kHz line broadening of the proton spectrum is understood from several points of view, namely, (1) that the proton line shape captures a much larger fraction of the total signal with a correspondingly larger average electron−nuclear dipolar interaction than does the ^{13}C line shape, (2) the static, thermally averaged electron moment is 3 times larger at 7.05 T compared to 2.35 T, (3) the gyromagnetic ratio of the protons is 4 times that of the carbons, and (4) the presence of MAS at 2.35 T results in some partial averaging of line width compared with the use of a static sample at 7.05 T.) (D) CRAMPS spectra (not shown), using the MREV-8 sequence and a 1.5-ms 90° pulse with a cycle time of 38.4 ms, are quite usual for the Laponite, showing [modest chemical shift resolution at a MAS frequency of 2.5 kHz. In contrast, the CRAMPS spectrum of the treated montmorillonite under the same conditions is extremely weak, even vanishing for a nonspinning sample. The latter observations are consistent with strong static dipolar couplings between the electrons and protons (only partially averaged in the MREV-8 sequence) as well as significant magnetic fluctuations in the mid-kHz range (thereby interfering with multiple-pulse averaging). (E) Finally, direct $T_{1\rho}{}^{H}$ measurements, utilizing a nutation frequency of 60 kHz, give average $T_{1\rho}{}^{H}$'s of 2.2 ms (70 μs) when total integrals are plotted. (All of the $T_{1\rho}{}^{H}$ plots show some deviation from single-exponential behavior; hence, there is certainly a distribution of intrinsic $T_{1\rho}{}^{H}$'s, as would be expected of protons with a range of distances to the nearest paramagnetic center and different electron−nuclear dipole−dipole interactions.)

The following commentary attempts to assign an order of magnitude to τ_e based on the observed $T_1{}^{H}$ of 4.7 ms for the OM in this particular clay. This $T_1{}^{H}$ of 4.7 ms implies[40] that the average τ_e is $<10^{-8}$ s because a τ_e of 10^{-8} s would give a $T_1{}^{H}$ at 300 MHz of 4.7 ms for a proton 0.6 nm away from a single Fe^{3+} ion. Considering the density of Fe^{3+} in the clay layer (discussed later) and the thickness of the layer containing the OM, we expect that most protons will be in the range from 0.6 to 1.1 nm away from the nearest Fe^{3+} atom, that is, at distances greater than 0.6 nm. In addition, the distribution of correlation times is probably broader than assumed in the above calculation (as evidenced by the short 70-μs $T_{1\rho}{}^{H}$, which in turn, implies a significant spectral density in the mid-kHz range). Both the distance range and the spectral broadness would require that the mean value of τ_e decrease toward the τ_e value at the $T_1{}^{H}$ minimum, namely, $\tau_e = 5.3 \times 10^{-10}$ s. On the other hand, contributions from multiple neighboring Fe^{3+} sites are probably not negligible. Taking all of the foregoing into consideration, the 4.7-ms $T_1{}^{H}$ implies that, at 7.05 T, τ_e is conservatively in the range 10^{-8} s $> \tau_e > 3 \times 10^{-11}$s. Thus, τ_e is indeed in the vicinity of the Larmor frequency for the protons and ^{13}C nuclei; hence, *we can expect a substantial direct influence on*

the $T_1{}^{H}$'s of all the protons within about 1 nm of a clay surface (and an associated, indirect, spin-diffusion-mediated influence on spins 20−30 nm from the clay surface...a topic treated in the second paper in this series).

The presence of the strong coexisting mid-kHz fluctuations contributes to the ineffectiveness of multiple-pulse line narrowing and the poor CRAMPS performance. Relative to that averaging, however, the presence of multiple, albeit weak, spinning sidebands in spectra taken with 5-kHz MAS (Figure 7) indicates that for those protons, which are probably both most mobile and in locations most dilute in Fe neighbors, MAS can average away, on a time scale of about 100 μs, a significant portion of the electron−nuclear dipolar interaction. This latter observation lends some validity to the approach of Yang and Zax[8] in attributing line broadening for nuclei close to the montmorillonite surface as solely arising from interactions with the thermally averaged, static, electron dipolar fields. However, given the very short $T_{1\rho}{}^{H}$'s that we observe, there will also be an associated, non-negligible, dynamic line broadening that would arise from these strongly fluctuating dipolar fields. We will not pursue question of the precise line width contributions from the static and dynamic dipolar fields; it is sufficient for our purposes to recognize that, within 0.4 nm of a clay surface, both influences are very important.

To summarize the observations for comparing the diamagnetic and paramagnetic organically modified clays, the influence of the paramagnetic iron at 2.35 T is to (a) cause a signal loss of about two-thirds in the 25-MHz ^{13}C Bloch-decay spectra, (b) cause a $200-250$-Hz broadening of the residual observable ^{13}C signals at a MAS frequency of 4 kHz, and (c) cause a major reduction in $T_{1\rho}{}^{H}$ so as to make the ^{13}C CPMAS spectra of these surface molecules very nonquantitative. Also, the molecules at the surface of the Laponite clay show large-amplitude mobility, even though they are tethered to the surface. At 7.05 T, the influence of the unpaired electrons on the protons is to (a) cause a signal loss of about one-third, (b) shorten $T_1{}^{H}$ by a factor of about 35, (c) cause a line broadening, having some *inhomogeneous* character, up to at least 30 kHz, (d) shorten $T_{1\rho}{}^{H}$ by a factor of about 30, and (e) make observable CRAMPS intensities very weak and very dependent on ν_r. It is clear that if one were interested in directly observing molecules at the clay surface, for example, monitoring chemical changes of the OM, one would have to use a diamagnetic clay, such as Laponite. There is too much loss of resolution and quantitation at the paramagnetic montomorillonite surface.

In their study[8] of montmorillonite clays that were intercalated with Li^+-doped poly(ethylene oxide), Yang and Zax took into account all the Fe sites within a radius of 2.5 nm when computing the Li NMR line shapes. In that system, the layer spacing was also 1.8 nm. Applying the same criterion to our treated clays, we should mainly be taking into account nearby Fe ions in both the clay layers that define the gallery bracketing the nucleus of interest. However, in the exfoliated NnC's, those nuclei that are close to a clay layer only see the broadening from the Fe ions in a single layer; the next layer is too distant. Therefore, *the impact of*

the Fe ions on the nuclei in the OMCs should be considered as an upper limit for the impact that Fe ions will have on corresponding nuclei that lie within 0.4 nm of the clay layers in exfoliated NnC's.

Discussion

It is well-recognized that the presence of clay promotes the formation of the γ-phase of nylon-6. Studies indicate[32,45] that the chain axes of the γ-crystallites are parallel to the clay surfaces in thinner films. Also, either the zigzag plane of the molecule or the H-bonding sheet plane is parallel to the clay surfaces.[32] The crystal growth direction is not specified; however, the model proposed by Fujimoto et al.[45] indicates growth normal to the clay surface. The generality of the foregoing studies is questioned in the study of a 3-mm-thick, injection-molded bar (mold temperature 60 °C) of an IsP NnC. There, the chain axes of the γ-crystallites were found[46] to be parallel to the clay layers only to a depth of about 0.5 mm from the bar surface. Below this level, the chain axes became perpendicular to the clay surfaces. This change in orientation was attributed to the different shear-stress histories at the different depths with the perpendicular orientation expected in the case of histories of lower shear stress. Because of the limited thickness of nylon-6 crystallites (deduced herein to be $\approx$6 nm) and because the growth direction is generally normal to the chain axes, the process of propagating the growing γ-crystallites so as to fill the region between the clay platelets ($\Delta \approx 40-50$ nm) seems more complicated to visualize when the chain axes are perpendicular to the clay surfaces and the initial growth direction is parallel to these surfaces.

Our DSC data as well as data of others[45] certainly demonstrate that the γ-phase nucleation by the clay occurs at a higher temperature than the α-phase nucleation in pure nylon-6. The fact that one can produce dominant γ-phase crystallites in a nylon-6 sample having <0.2% clay[33] indicates that the γ-phase growth propagates from the surface of the clay for fairly long distances ($\approx$500 nm). That seems to us more consistent with the notion of an initial growth direction perpendicular to the clay surface unless there is some mechanism for facile changes in the direction of γ-crystal (versus α-crystal) growth.

In terms of comparative crystal structures, the α- and the γ-crystallites have their interchain H-bonding confined to sheets in whose planes the chain axis also resides. An interesting difference between the α- and γ-phase crystallites is that, in the plane of these sheets, all chains are pairwise antiparallel in the α-crystallites and fully parallel in the γ-phase. What is not agreed upon, for the γ-phase crystal structure, is whether the direction of the chains in adjacent sheets is alternating and ordered[10] or simply disordered.[11] In any case, γ-phase crystallites are thought to be made up of about equal numbers of chains with the two directionalities; otherwise, it would be a difficult topological problem to explain the solid-state transformation from the α- to the γ-phase upon exposure to a 1.2 N I₂/KI aqueous iodine

solution.[47] The foregoing considerations suggest that differences in the structure of the NC regions, for samples dominated by either the α- or the γ-phase crystallites, are probably minimal because chain folding can be, in principle, accommodated in both lattices.

Note that the clay nucleates the γ-form in all the materials we investigated, that is, in both blended and IsP NnC's. So covalent attachment of the nylon to the surface of the clay, characteristic of the latter NnC's, is not the most critical issue for nucleating the γ-crystallites, even though one might be tempted to argue that the formation of parallel-chain sheets is promoted because there is a preordering of chain directionality at the clay surface. (The chemistry of attachment is specific to the amine end of the molecule.) Arguments for this latter mechanism of nucleation are, however, further weakened by the requirement that the γ-phase crystallites require frequent directional changes for adjacent H-bonded sheets and that the chain-axis direction is, under certain circumstances, found to be parallel, not perpendicular, to the clay surface. Also, in a study[7] of the impact of clay layers on the organization of nylon-6 crystallites at 205 °C, it was observed that, compared to the case of blended nylon-6/clay NnC's, the crystallites that formed for IsP NnC's were less perfect. The suggestion put forth[7] was that the constraints imposed by tethering were, at least at elevated temperatures, more disruptive to crystallite organization than were the weaker interactions of blended chains with the clay surfaces. Nevertheless, for both types of NnC's, γ-phase crystallites are dominant.

Processing temperature is an important consideration because it can relate to chemical stability and microstructural reproducibility. From a practical point of view, the NnC's have a higher effective melt viscosity than the pure nylon-6. Hence, the tendency is to lower the viscosity by processing these materials at higher temperatures than nylon-6 would be processed. The choice of 295 °C as a processing temperature for the injection-molded N6C-Is-M samples is not an unusually high processing temperature for this NnC. In this context, it is very significant, in our opinion, that this processing history is accompanied by irreversible changes for the IsP samples. The irreversibility is seen most prominently in the large difference in the f_α values, respectively 0.63 and 0.12, for samples N6C-Is-M-e and N6C-Is-M-h. These samples were both slowly cooled from the melt (yielding comparable and low f_α values) with subsequent annealing at 214 °C for about 18 h. The difference is that the former sample had a prior history of being injection-molded at 295 °C. While we cannot specify in detail what those irreversible changes are, it is clear that, during annealing, the stability of the γ-crystallites changed dramatically, despite the uniform melt-crystallization histories. The only hypotheses we have to explain this phenomenon are (a) a degradation of molecular mass of the nylon-6 during the 295 °C injection-molding process so that there would be extensive, albeit partial, melting during annealing, especially in regions more distant from the clay surfaces, and/or (b) a significant chemical alteration of the clay surfaces during the 295 °C injection-molding process

(45) Fujimoto, K.; Yoshikawa, M.; Katahira, S.; Yasue, K. *Kobushshi Robunshu,* **2000**, *57*, 433.

(46) Kojima, Y.; Usuki, A. Kawasumi, M.; Okada, A.; Kurauchi, T.; Kamigaito, O.; Kaji, K. *J. Polym. Sci.(B), Polym. Phys.* **1995**, *33*, 1039.

(47) Ueda, S.; Kimura, T. *Kobunshi Kagaku* **1958**, *15*, 243.

with the result that the γ-phase could not be as efficiently stabilized by the surface interactions during annealing. For example, if the surface lost its affinity for the nylon-6, then the surface would exert less influence for stabilizing the γ-crystallites. Choosing between these possibilities or identifying another possibility awaits further experimentation. It may be worth noting, however, that the 6-mm-o.d. machined samples, made from the injection-molded NnC, maintained their dimensional tolerances to within 0.03 mm after annealing, despite being laterally unsupported during annealing. Hence, if melting occurred during annealing, it was probably never extensive at any given time. Also note that the blended NnC's were not subjected to the 295 °C injection molding so it is inappropriate to conclude that the irreversible changes are only associated with the IsP NnC's.

We can, at this time, only speculate on the importance of the partitioning of the crystalline phases between the α- and γ-forms. A change in the γ/α ratio might, by itself, have a modest impact on mechanical properties either by altering the crystal modulus (supposing that the two forms have different moduli). Crystallite orientation relative to clay orientation is also of potential importance. Processing-induced chemical degradation at the interface might lead to changes in the crystal growth direction or in the affinity of the clay surface for the polymer, thereby influencing properties.

In terms of any widespread changes in polymer dynamics or morphological organization associated with the presence or absence of the clay, the significant measurements relating to dynamics involved comparing $T_{1\rho}{}^H$ data for NnC's and for nylon-6. Contrasts in $T_{1\rho}{}^H$ behavior were negligible, although most of the protons sampled were more than 2 nm from any clay surface. In addition, we report that the T_{1xz} profiles, for pairs of N6 and N6C-B-L1 samples with similar thermal histories, were very similar (not shown). Because T_{1xz} is associated with the superposition of site-specific decay rates, in contrast to the spin-diffusion averaging of $T_{1\rho}{}^H$, this observation underscores the similarity of mobility, particularly in the NC regions of N6 and the NnC's. Morphologically, there were no significant changes in the average domain sizes between those NnC's and nylon-6 that had the same (slow-cooling) thermal histories. In fact, even though there were modest increases in crystallinity as a result of annealing, there was no significant change in the "long period". Thus, at distances greater than, say, 2 nm from the clay surfaces, the clay seemed to have no significant impact on dynamics or morphology, outside of modifying the dominant CR form. Morphological changes upon annealing were only local...occurring within dimensions of the long period. Our finding that the crystallinity of the NnC was very similar to that of pure N6 has also been reported by others.[32] In view of the reported[7] negative impact that tethering had on the high-temperature organization of crystallites in IsP NnC's, we will not claim, in the absence of experiment, that the ambient-temperature morphological similarity observed between nylon-6 and the blended NnC's carries over to the IsP NnC's.

The influence of Fe^{3+} in the clay layers on spins within about 0.4 nm of the clay surface is, in part,

consistent with the line width perturbation from partially polarized electrons...an effect treated by Yang and Zax.[8] However, other phenomena, such as signal disappearance, and the dramatic shortening of both $T_1{}^H$ and $T_{1\rho}{}^H$ are additional, important perturbations on the nuclear spins that were not treated by Yang and Zax. On the one hand, it will be very difficult to obtain resolution and quantitation of NMR signals for spins within, say, 1 nm of montmorillonite clay surfaces. On the other hand, the recognition that the unpaired electrons on Fe^{3+} in these montmorillonite clays have near optimum spectral density for inducing very efficient $T_1{}^H$ relaxation for nearby protons provides the rationale (along with the concept of spin diffusion) for using $T_1{}^H$ measurements as relative assays of the quality of montomorillonite clay dispersion in these NnC's. This topic will be treated in the second paper in this series.[15]

Conclusions

We have looked at several, nominally 95/5 nylon-6/montmorillonite-clay nanocomposites (NnC's) made by both blending and in situ polymerization. The well-known phenomenon that the presence of the clay promotes the formation of the γ-phase of nylon-6, in contrast to the usual α-phase of pure nylon-6, was observed. The fraction of γ-phase was also observed to decrease with increasing cooling rate for a given NnC. DSC indicated that crystal nucleation takes place in the NnC at a temperature significantly higher than that of the nylon-6; thus, the dominance of the γ-phase is, in part, related to the fact that the γ-phase growth from the clay surface obtains a head start on any growth of the α-phase originating in regions away from the clay surface. For slowly cooled (SC) samples, cooled at 1 °C/min from the melt, the γ-phase was the dominant crystal phase for both blended (B) and in situ polymerized (IsP) samples. Moreover, for annealing cycles at 214 °C for several hours using a slow approach to the annealing temperature, the γ-phase of the SC samples showed only a minor amount of conversion from γ to α. The exception to this was an IsP sample, injection-molded at 295 °C, where a much larger fraction of the crystallites converted from γ to α. Thus, some irreversible changes take place during injection molding at 295 °C, originating most likely from either a degradation of molecular mass or from changes in the chemistry of the polymer/clay interface.

The use of paramagnetic montmorillonite clays for NnC formulations was seen as an opportunity to deduce useful information. We studied the direct influence of the paramagnetic Fe^{3+} ions on protons and ^{13}C nuclei within 0.4 nm of clay surfaces by looking at organically modified clays. It was seen that the electron−nuclear interactions over these short distances caused substantial signal loss, in addition to which both the longitudinal and the rotating-frame relaxation times were strongly modified. These perspectives helped us to understand properly the $T_1{}^H$ behavior of the nylon protons in exfoliated NnC's, a topic more fully explored in the second paper in this series.

No significant difference in overall morphological repeat distance, crystallinity, or average mobility of the

noncrystalline segments was detected in a diamagnetic blended NnC relative to the pure nylon-6. These comments should carry over to paramagnetic blended NnC's; however, we are withholding judgment with regard to IsP NnC's. Certainly, the comparable $T_{1\rho}^{H}$ behaviors for all NnC's and nylon-6 suggest very similar mobility of the NC segments.

CM0110775